Assessment of Multivariate Information Transmission in Space-Time-Frequency Domain: A Case Study for EEG Signals

Sixuan He, Yaru Li, Xinning Le, Xiaoyu Han, Jingfeng Lin, Xiaohang Peng, Min Li, Ruobing Yang, Dezhong Yao, Pedro A. Valdes-Sosa, and Peng Ren

***Abstract*— Objective: Multivariate signal (MS) analysis, especially the assessment of its information transmission (for example, from the perspective of network science), is the key to our understanding of various phenomena in biology, physics and economics. Although there is a large amount of literature demonstrating that MS can be decomposed into space-time-frequency domain information, there seems to be no research confirming that multivariate information transmission (MIT) in these three domains can be quantified. Therefore, in this study, we attempted to combine dynamic mode decomposition (DMD) and parallel communication model (PCM) together to realize it. Methods: We first regarded MS as a large-scale system and then used DMD to decompose it into specific subsystems with their own intrinsic oscillatory frequencies. At the same time, the transition probability matrix (TPM) of information transmission within and between MS at two consecutive moments in each subsystem can also be calculated. Then, communication parameters (CPs) derived from each TPM were calculated in order to quantify the MIT in the space-time-frequency domain. In this study, multidimensional electroencephalogram (EEG) signals were used to illustrate our method. Results: Compared with traditional EEG brain networks, this method shows greater potential in EEG analysis to distinguish between patients and healthy controls. Conclusion: This study demonstrates the feasibility of measuring MIT in the space-time-frequency domain simultaneously. Significance: This study shows that MIT analysis in the space-time-frequency domain is not only completely different from the MS decomposition in these three domains, but also can reveal many new phenomena behind MS that have not yet been discovered.**

***Index Terms*— Dynamic mode decomposition (DMD), electroencephalogram (EEG), multivariate information transmission (MIT), multivariate signal (MS), network science, space-time-frequency, parallel communication model (PCM).**

Manuscript received 21 September 2022; revised 29 January 2023; accepted 13 March 2023. Date of publication 21 March 2023; date of current version 28 March 2023. This work was supported in part by the National Natural Science Foundation of China under Grant 62171109, Grant 82121003, and Grant 81871446; in part by the Sichuan Science and Technology Program under Grant 2020YFS0094; and in part by the Chengdu Science and Technology Bureau Program under Grant 2022-GH02-00042-HZ. *(Corresponding authors: Pedro A. Valdes-Sosa; Dezhong Yao; Peng Ren.)*

Sixuan He, Yaru Li, Xinning Le, Xiaoyu Han, Jingfeng Lin, Xiaohang Peng, Min Li, Pedro A. Valdes-Sosa, and Peng Ren are with Sichuan Provincial People's Hospital, MOE Key Laboratory for Neuroinformation, School of Life Science and Technology, University of Electronic Science and Technology of China, Chengdu 611731, China (e-mail: pedro@uestc.edu.cn; pren28@uestc.edu.cn).

Ruobing Yang is with the Department of Communication Engineering, School of Information and Communication Engineering, University of Electronic Science and Technology of China, Chengdu 611731, China.

Dezhong Yao is with Sichuan Provincial People's Hospital, MOE Key Laboratory for Neuroinformation, School of Life Science and Technology, University of Electronic Science and Technology of China, Chengdu 611731, China, and also with the Research Unit of NeuroInformation, Chinese Academy of Medical Sciences, 2019RU035, Chengdu 610041, China (e-mail: dyao@uestc.edu.cn).

Digital Object Identifier 10.1109/TNSRE.2023.3260143

I. Introduction

A. Introduction to Multivariate Information Transmission

MULTIVARIATE signal (MS) analysis is a mainstream topic across the scientific community, as well as a powerful method to describe the dynamics of complex systems [1]. Since these recorded signals are usually not completely independent, but interact with each other, it is of great significance to investigate the information transmission between them, and the method based on network science has become the leading approach. It has not only contributed to a better understanding of various phenomena in the fields of biology, economy, ecology, climate and transportation, but also has many practical applications [2]. For example, Zhang et al. used network science techniques to investigate multi-channel electrocardiograms in healthy subjects and patients with arrhythmia in order to enhance the accuracy rate of disease identification [3]. Mutua et al. proposed an approach called the visibility graph to analyze multivariate empirical records from stock markets; the results showed that this network method can provide valuable future stock price predictions [4]. Deza et al. used network science to study historical temperature records from multiple locations around the world, and revealed the inherent dynamics of the global climate [5]. Tang et al. employed correlation coefficients on multiple traffic time series to construct a network, and concluded that the periodicity of traffic data can efficiently predict traffic patterns over the course of a day [6]. Although network science can reveal topological connectivity between signals, it can only manifest multivariate information transmission (MIT) in the spatial domain, without considering their temporal and frequency domain properties. It is well known that MS contains three domains of information: space, time, and frequency. Nevertheless, it seems that no research to date has been able to successfully quantify how multivariate

information is transmitted simultaneously across these three domains. Aiming to rectify this deficiency, we attempted to combine dynamic mode decomposition (DMD) with a parallel communication model (PCM) to realize it. In addition, multidimensional electroencephalogram (EEG) signals were employed as an example to illustrate our method.

The contributions of this article are as follows: (1) As shown in Table I in the Appendix, traditional network analysis is able to describe MIT and quantify it with topological parameters, but this approach only reveals the spatial information of MS. In addition, although tensor analysis can decompose MS in three domains, it cannot describe how MS transmit information simultaneously in these domains [7]. Only our proposed approach can quantitatively evaluate MIT in the space-time-frequency domain. In our method, DMD was first employed to unveil the MIT in the space-time-frequency domain, and then parameters extracted from the PCM model were used to quantify MIT [8], [9]. (2) Unlike previous literature, our method does not regard MS as a closed system, but rather as an open system; they constantly exchange information with the outside environment. In this paper, EEG signals were used as an example to illustrate this method. The brain, as commander-in-chief of the body, constantly interacts with other physiological systems (such as the circulatory and respiratory systems). Therefore, it is unreasonable to regard EEG signals as a closed system as a description of its functional activities. Our approach not only attempts to describe information transmission within the brain, but also reveals how the brain transmits information to other physiological systems, and vice versa. (3) Our method extracts a series of parameters which can reveal new phenomena behind MS. For example, the channel capacity parameter is used to explore the maximum information transmission capacity of the brain, and further investigate whether the disease significantly alters this capacity. This question has never been studied and answered.

B. Background Description

1) Multidimensional EEG: Multidimensional EEG is one of the most important imaging modalities in neuroscience, owing to its low cost, non-invasive, simple acquisition and high (millisecond-level) temporal resolution advantages. EEG is collected primarily by placing standardized, conductive, and multichannel electrodes on the surface of an individual's skull [10]. At present, there are many ways to analyze multichannel EEG signals, among which the brain network (BN) method is the most commonly employed. For example, Jalili et al. constructed EEG BN using partial correlation (PC) and then investigated its small-world, vulnerability, modularity, assortativity and synchronizability to distinguish schizophrenia patients from healthy controls (HC) [11]. Deng et al. constructed BN based on the phase locking value (PLV) of each pair of EEG signals, and then extracted their corresponding topological attributes for emotion recognition [12]. Nicolaou and Georgiou calculated the Granger causality (GC) of each pair of EEG signals to construct BN in order to automatically classify the states of general anesthesia patients between awake and anesthesia [13]. It is worth noting that although the application of BN in multidimensional EEG signal analysis can be used to reveal the functional connections between different brain regions, the above three defects still exist [14], [15], [16]. Therefore, we attempted to quantify how EEG signals simultaneously transmit information in the space-time-frequency domain by the combination usage of DMD and PCM.

2) Dynamic Mode Decomposition: DMD was originally used for fluid flow analysis, and recently implemented to investigate high-dimensional physiological signals, such as EEG signals. It can capture their coherent spatiotemporal patterns without making any prior assumptions [17], [18]. Furthermore, DMD is able to decompose EEG signals into subsystems with their own intrinsic oscillatory frequency, which provides a way to investigate how EEG signals transmit information at different frequencies [19]. Simultaneously, their corresponding transition probability matrices (TPM) are also calculated to describe the spatio-temporal information transmission within and between signals of each subsystem.

3) Communication Model: A basic communication model usually consists of three indispensable parts: the senders (or sources), the receivers (or sinks), and the communication channel that carries information from the senders to the receivers [20]. The communication channel determines the basic nature of the model and usually is the most important of these components [21]. In mathematical expression, a TPM is usually implemented to describe the properties of the communication channel, whose rows and columns respectively indicate the senders and receivers. Each element in the matrix represents the probability that a receiver gets the message when a given sender emits it [22]. In general, a series of communication parameters (CPs) can be obtained through the TPM in order to quantify MIT in the model.

It should be noted that in practical applications, communication systems are usually large in scale and must be decomposed into multiple parallel subsystems to realize information transmission; that is, a PCM is adopted [23]. Generally, the PCM subsystems are not only independent of one other, but also can deliver information within their own specific frequency bands; that is, the frequency band of the whole system is divided into sub-frequency bands overlapping in time but not in frequency, in order to ensure the efficiency of MIT in the whole communication system.

In this study, all EEG leads (i. e. brain regions) are regarded as both senders and receivers in the communication model. Communication channels are regarded as the vehicle, by which the information is transmitted between leads. Furthermore, many studies have demonstrated that the brain is composed of many dynamic subsystems, which provides physiological basis to investigate EEG signals using PCM. It should be pointed out that the method of DMD was employed first to extract EEG dynamic subsystems for further CP extraction in order to quantify MIT in the space-time-frequency domain.

4) Assessment of MIT for EEG Signals in the Space-Time-Frequency Domain: This study uses patients with Parkinson's disease (PD) as an example of EEG signals to illustrate the proposed approach. The main symptoms of PD patients include not only motor symptoms, but also non-motor symptoms, such as cognitive dysfunction [24]. Many previous

studies have employed EEG signals to investigate the brain function of PD patients. For example, Li et al. revealed that EEG BN in PD patients can be implemented to predict the severity of gait freezing [25]. Geraedts et al. showed that analysis of EEG BN of PD patients can be used for effective early diagnosis of their non-motor symptoms [26]. Olde Dubbelink et al. showed that EEG BN decentralization is an early symptom of PD patients, and suggested that the severity of the disease increases over time in patients with strong decentralization [27]. Although these traditional BN approaches can reveal the brain information transmission process of PD patients to a certain extent, as mentioned above, some deficiencies still remain. Therefore, this study attempts to implement the DMD-based PCM to investigate the MIT of EEG signals for PD patients.

In this paper, PCM is used for EEG analysis; its working diagram is shown in Fig. 1. First, multidimensional EEG signals were preprocessed for noise and artifact removal. Then, the preprocessed EEG signals were decomposed into subsystems with their own intrinsic oscillatory frequencies by DMD. At the same time, the TPM of information transmission within and between MS at two consecutive moments in each subsystem can also be calculated. In the following, CPs derived from each TPM were calculated, and distribution indexes (DI) for each type of CP in all EEG subsystems were derived within each EEG frequency band (delta, theta, alpha and beta waves) for further statistical testing and classification of PD and HC. The DMD-based PCM model developed in this paper is illustrated above. Furthermore, two other types of methods, namely the unparallel communication model (UCM) without subsystem decomposition and traditional BN methods, were also employed for comparison. It is worth noting that DMD-based PCM quantitatively measures MIT in the space-time-frequency domain, while UCM only describes MIT in the spatio-temporal domain, and BN only investigates MIT in the spatial domain.

II. Materials and Methods

A. Dataset Collection and Preprocessing

This study used the well-known public dataset "Parkinson's disease: Resting state EEG (https://osf.io/pehj9/)" for analysis. The dataset includes 20 PD patients (ages: 70.0 ± 7.2 years, 9 males and 11 females) and 20 age-matched control participants without neurological disease (ages: 68.0 ± 6.0 years, 8 males and 12 females). All PD patients were diagnosed using the UK Brain Bank (or Movement Disorder Society) clinical criteria. The Unified-Parkinson Disease Rating Scale (UPDRS) scores of these PD patients are 28.9 ± 16.9. The experiment was approved by the Ethics Committee of the Hospital District of Southwest Finland, and conducted according to the principles of the Declaration of Helsinki. EEG signals were recorded with 64 electrodes by a NeurOne (Bittium, Finland) Tesla amplifier (sampling rate: 500 Hz, bandpass filtering: 0.16 to 125 Hz). The resting EEG signals of each subject with eyes closed were collected for two minutes. Data preprocessing was performed using PREP, a well-known toolbox for large-scale EEG signal preprocessing [28].

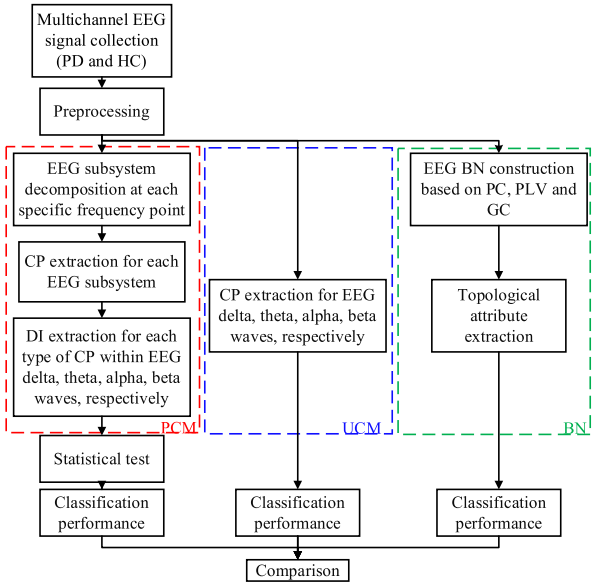

Fig. 1. Flow chart of this paper. Note: PCM, UCM, and BN denote the parallel communication model, unparallel communication model, and brain network, respectively. The UCM was constructed directly based on the EEG delta, theta, alpha and beta waves, without any subsystem decomposition. The BNs were constructed via PC, PLV and GC. The topological attributes of BN include the clustering coefficient, rich club coefficient, network density, network strength and average link strength. Finally, accuracy, precision, recall, and area under the receiver operator characteristic curve (AUC) were regarded as classification performance indexes to evaluate the differentiation ability of the two-subject groups.

It performs automated noise removal, bad channel detection, and referencing in a way that allows users to divert the data to particular applications without any direct operations on the raw data.

B. EEG Subsystem Decomposition Based on DMD

DMD is a data-driven method which decomposes EEG signals into dynamic modes (DMs) in the form of spatio-temporal coherent structures, which can be seen as subsystems of the signal [29]. This algorithm focuses on finding a linear operator $\mathbf{A}$ by way of linear regression between $\mathbf{X}^{pri}$ and $\mathbf{X}^{pos}$, which satisfies the following equation:

$$\mathbf{X}^{pos} = \mathbf{A}\mathbf{X}^{pri} \tag{1}$$

$$\mathbf{X}^{pri} = \begin{bmatrix} | & | & & | \\ \mathbf{x}_1 & \mathbf{x}_2 & \cdots & \mathbf{x}_{t-1} \\ | & | & & | \end{bmatrix} \tag{2}$$

$$\mathbf{X}^{pos} = \begin{bmatrix} | & | & & | \\ \mathbf{x}_2 & \mathbf{x}_3 & \cdots & \mathbf{x}_t \\ | & | & & | \end{bmatrix} \tag{3}$$

where $\mathbf{X}^{pri}$ and $\mathbf{X}^{pos}$ are two $n \times (t\text{-}1)$ matrices, n and t indicate the number of EEG leads and number of EEG sampling points, respectively. Specifically, $\mathbf{X}^{pri}$ and $\mathbf{X}^{pos}$ represent the multidimensional EEG data collected from time point 1 to t-1, and from time point 2 to t-1, respectively, regarded as the EEG signals recorded in the prior and posterior time periods. It is not practical to directly calculate operator $\mathbf{A}$entirely from $\mathbf{X}^{pri}$ and $\mathbf{X}^{pos}$, because n is too

large to perform the eigen-decomposition of $\mathbf{A}$, which would have a prohibitively high computational cost. Therefore, the DMD algorithm employed a rank-reduced approach, where the eigenvalues and eigenvectors of $\mathbf{A}$ were calculated by the low-rank approximate matrix $\tilde{\mathbf{A}}$. The specific steps are shown as follows.

Step 1. Use singular value decomposition on $\mathbf{X}^{pri}$:

$$\mathbf{X}^{pri} \approx \mathbf{U}\Sigma\mathbf{V}^* \tag{4}$$

where $\mathbf{U}$ and $\mathbf{V}$ represent the left and right singular vectors of $\mathbf{X}^{pri}$, respectively, and the asterisk represents a conjugate transpose.

Step 2. Substitute (4) into (1) and rewrite $\mathbf{X}^{pos}$:

$$\mathbf{X}^{pos} = \mathbf{A}\mathbf{U}\Sigma\mathbf{V}^* \tag{5}$$

Step 3. Project $\mathbf{A}$ on $\mathbf{U}$ to obtain the low-rank matrix $\tilde{\mathbf{A}}$:

$$\tilde{\mathbf{A}} \triangleq \mathbf{U}^*\mathbf{A}\mathbf{U} = \mathbf{U}^*\mathbf{X}^{pos}\mathbf{V}\Sigma^{-1} \tag{6}$$

Step 4. Calculate the eigen-decomposition of $\tilde{\mathbf{A}}$:

$$\tilde{\mathbf{A}}\mathbf{W} = \mathbf{W}\Lambda \tag{7}$$

where $\mathbf{W}$ is the matrix of eigenvectors of $\tilde{\mathbf{A}}$, and Λ is the diagonal matrix containing all eigenvalues λ_m $(m = 1, \ldots, r)$.

Step 5. Compute the DMs (i.e. the eigenvectors of $\mathbf{A}$):

$$\mathbf{\Phi} = \mathbf{X}^{pos}\mathbf{V}\Sigma^{-1}\mathbf{W} \tag{8}$$

Each column of $\mathbf{\Phi}$, namely $\boldsymbol{\phi}_m$, accompanied by the corresponding eigenvalue λ_m, represents the eigenvectors of $\mathbf{A}$ [17], [18]. The value of m ranges from 1 to r, and r is set to 300, representing the number of truncated modes (i.e. number of DMs). For more details about the r value, refer to the discussion. Apart from this, each DM $\boldsymbol{\phi}_m$ contains n elements, indicating the power amplitude values of n EEG leads in the m^{th} DM, respectively. It is expressed as follows:

$$\boldsymbol{\phi}_m = [\phi_m^1, \ldots, \phi_m^i, \ldots, \phi_m^n]^T \tag{9}$$

Furthermore, the oscillatory frequency of the DM $\boldsymbol{\phi}_m$ can be calculated from its corresponding eigenvalue λ_m:

$$f_m = \left| \frac{imag\left(\log(\lambda_m)/\Delta t\right)}{2\pi} \right| \tag{10}$$

where Δt indicates the time difference between two sequential sampling time points of the signal [20]. Finally, the linear operator $\mathbf{A}$ can be estimated as follows:

$$\mathbf{A} = \mathbf{\Phi}\Lambda\mathbf{\Phi}^{\dagger} \approx \sum_{m=1}^{r} \boldsymbol{\phi}_m \lambda_m \boldsymbol{\phi}_m^{\dagger} \tag{11}$$

where '†' means the pseudoinverse. Then, the sublinear shift operator $\mathbf{A}_m$ can be easily derived as follows:

$$\mathbf{A}_m = \boldsymbol{\phi}_m \lambda_m \boldsymbol{\phi}_m^{\dagger} \tag{12}$$

which describes how EEG signals at a particular frequency f_m are transmitted within the m^{th} DM (i.e. subsystem). These DMs not only represent spatio-temporal patterns [19], but also correspond to specific frequencies f_m. As can be seen, DMD provides the foundations to investigate multidimensional EEG signals from the space-time-frequency perspective.

It should be noted that in practical application, we often use the augmented matrices $\mathbf{X}_{aug}^{pri}$ and $\mathbf{X}_{aug}^{pos}$, rather than $\mathbf{X}^{pri}$ and $\mathbf{X}^{pos}$, to obtain the sublinear operator $\mathbf{A}_m$. The shift-stacked data matrix method introduced by Tu et al., was used to obtain the augmented matrices. Please refer to [30] for details.

C. EEG Analysis Based on Parallel Communication Model

As mentioned above, each EEG subsystem obtains one sublinear shift operator, $\mathbf{A}_m$. Then, its corresponding TPM $\mathbf{P}_m^{pos|pri}$ can be inferred as follows:

$$\begin{aligned}\mathbf{P}_m^{pos|pri} &= norm\left((\mathbf{A}_m)^T\right) \\ &= \begin{pmatrix} p_m\left(l_1^{pos}|l_1^{pri}\right) & \cdots & p_m\left(l_n^{pos}|l_1^{pri}\right) \\ \vdots & p_m\left(l_j^{pos}|l_i^{pri}\right) & \vdots \\ p_m\left(l_1^{pos}|l_n^{pri}\right) & \cdots & p_m\left(l_n^{pos}|l_n^{pri}\right) \end{pmatrix}\end{aligned} \tag{13}$$

$$p_m\left(l_j^{pos}|l_i^{pri}\right) \geq 0 \tag{14}$$

$$\sum_{j=1}^{n} p_m\left(l_j^{pos}|l_i^{pri}\right) = 1 \quad (i = 1, 2, \ldots, n) \tag{15}$$

In order to meet the requirements of the TPM in the communication model, we first took the transpose of $\mathbf{A}_m$, then normalized each row (see (14) and (15)). The rows and columns of this matrix represent the senders and receivers of the communication model, respectively. Each element $p_m\left(l_j^{pos}|l_i^{pri}\right)$ denotes the transition probability that information is delivered from the i^{th} EEG lead to the j^{th} lead within the m^{th} subsystem. As mentioned above, the EEG signal was analyzed by the PCM, and its global configuration can be seen on the left side of Fig. 2. The right side of Fig. 2 indicates how the EEG leads transmit information within one subsystem, namely, its corresponding TPM.

Furthermore, the power ratio of the i^{th} EEG leads to all EEG leads within the m^{th} subsystem can be calculated as follows, which is given as the source probability distribution:

$$\begin{aligned}\mathbf{P}_m^{pri} &= \left[p_m\left(l_1^{pri}\right), \ldots, p_m\left(l_i^{pri}\right), \ldots, p_m\left(l_n^{pri}\right)\right] \\ &= \left[\frac{\left(\boldsymbol{\phi}_m^1\right)^2}{\left\|\boldsymbol{\phi}_m\right\|^2}, \ldots, \frac{\left(\boldsymbol{\phi}_m^i\right)^2}{\left\|\boldsymbol{\phi}_m\right\|^2}, \ldots, \frac{\left(\boldsymbol{\phi}_m^n\right)^2}{\left\|\boldsymbol{\phi}_m\right\|^2}\right]\end{aligned} \tag{16}$$

where the total power of all EEG leads and the power of its i^{th} lead in the m^{th} EEG subsystem are $\left\|\boldsymbol{\phi}_m\right\|^2$ and $\left(\phi_m^i\right)^2$, respectively.

The joint probability matrix in the m^{th} EEG subsystem can be computed below:

$$\mathbf{P}_m^{pri,pos} = diag\left(\mathbf{P}_m^{pri}\right)\mathbf{P}_m^{pos|pri} \tag{17}$$

with the size of $n \times n$, which consists of elements $p_m\left(l_i^{pri}, l_j^{pos}\right)$ $(i, j = 1, \ldots, n)$.

Then, the receiver probability distribution in the m^{th} EEG subsystem can be calculated below:

$$\mathbf{P}_m^{pos} = \mathbf{P}_m^{pri}\mathbf{P}_m^{pos|pri} \tag{18}$$

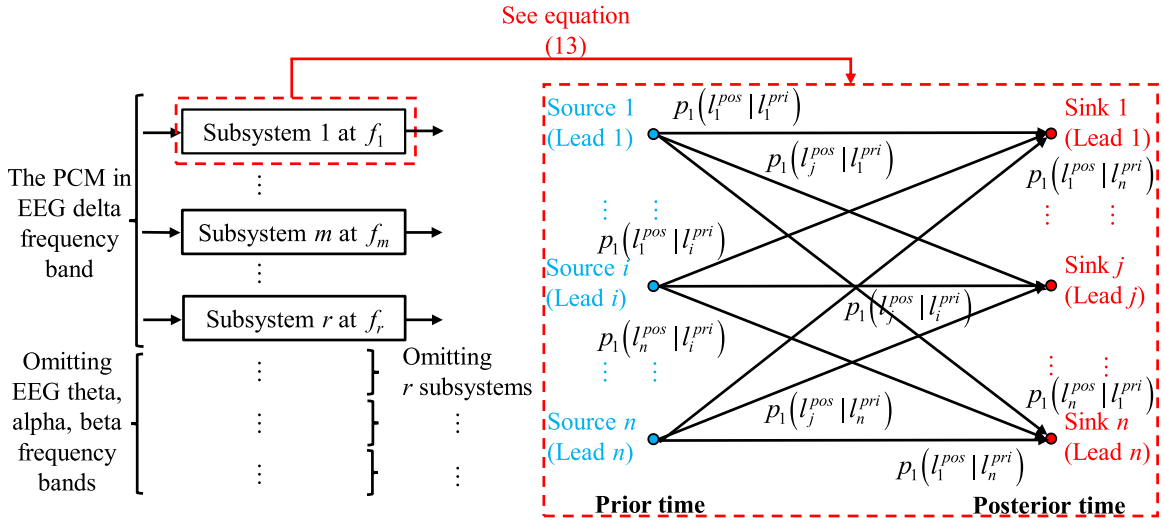

Fig. 2. The EEG signal was analyzed by the PCM; its configuration can be seen on the left side of the figure. The right side of the figure describes how each EEG lead transmits information in each subsystem, namely, its corresponding TPM. Note: f_m represents the intrinsic oscillatory frequency of the m^{th} subsystem.

with the size of $1 \times n$, which consists of elements $p_m\left(l_j^{pos}\right)$ $(j = 1, \ldots, n)$. Finally, another conditional probability matrix $\mathbf{P}_m^{pri|pos}$ in the m^{th} EEG subsystem can be computed by the division of $\mathbf{P}_m^{pri,pos}$ by $\mathbf{P}_m^{pos}$, with the size of $n \times n$, which consists of elements $p_m\left(l_i^{pri}|l_j^{pos}\right) = p_m\left(l_i^{pri}, l_j^{pos}\right) \Big/ p_m\left(l_j^{pos}\right)$ $(i, j = 1, \ldots, n)$ [20].

D. Feature Extraction

In this study, a total of 8 CPs was derived for each EEG subsystem, which are shown as follows:

1) Calculation for Each EEG Subsystem:

a) Source entropy: The source entropy of the m^{th} EEG subsystem is given below:

$$H_m^{pri} = -\sum_{i=1}^{n} p_m\left(l_i^{pri}\right) \log_2 p_m\left(l_i^{pri}\right) \tag{19}$$

which indicates the total amount of information contained within the m^{th} EEG subsystem, before any information is sent by brain regions.

b) Sink entropy: The sink entropy of the m^{th} EEG subsystem is given bellow:

$$H_m^{pos} = -\sum_{j=1}^{n} p_m\left(l_j^{pos}\right) \log_2 p_m\left(l_j^{pos}\right) \tag{20}$$

which indicates the total amount of information contained within the m^{th} EEG subsystem, after the information arrives at brain regions.

c) Loss entropy: The loss entropy of the m^{th} EEG subsystem is given below:

$$H_m^{pri|pos} = -\sum_{i=1}^{n}\sum_{j=1}^{n} p_m(l_i^{pri}|l_j^{pos}) \log_2 p_m(l_i^{pri}|l_j^{pos}) \tag{21}$$

which indicates the amount of information within the m^{th} EEG subsystem, sent by brain regions in the early stage, does not eventually reach themselves; that is, this part of the information is lost during the transmission process. This parameter may represent information transmitted by brain regions to the peripheral nervous system.

d) Degree of diffusiveness: The degree of diffusiveness in the m^{th} EEG subsystem is given below:

$$H_m^{pos|pri} = -\sum_{i=1}^{n}\sum_{j=1}^{n} p_m(l_j^{pos}|l_i^{pri}) \log_2 p_m(l_j^{pos}|l_i^{pri}) \tag{22}$$

which indicates the amount of information within the m^{th} EEG subsystem, received by brain region at a later time, does not originally come from themselves; that is, new information acquired during the transmission process. This parameter may represent information sent by the peripheral nervous system and eventually transmitted to brain regions.

e) Mutual information: The mutual information of the m^{th} EEG subsystem is given below:

$$I_m^{pri;pos} = \sum_{i=1}^{n}\sum_{j=1}^{n} p_m\left(l_i^{pri}, l_j^{pos}\right) \log_2 \frac{p_m\left(l_j^{pos}|l_i^{pri}\right)}{p_m\left(l_j^{pos}\right)} \tag{23}$$

which indicates the amount of information within the m^{th} EEG subsystem, transmitted between brain regions.

The relationship between these five types of CPs is shown in Fig. 3.

f) Joint entropy: The joint entropy of the m^{th} EEG subsystem can be derived from the five types of CPs mentioned above:

$$\begin{aligned} H_m^{pri,pos} &= H_m^{pri} + H_m^{pos|pri} \\ &= H_m^{pos} + H_m^{pri|pos} \\ &= H_m^{pri} + H_m^{pos} - I_m^{pri;pos} \end{aligned} \tag{24}$$

g) Channel capacity: The channel capacity of the m^{th} EEG subsystem is given below:

$$C_m = \max_{\mathbf{P}_m^{pri}} I_m^{pri;pos} \tag{25}$$

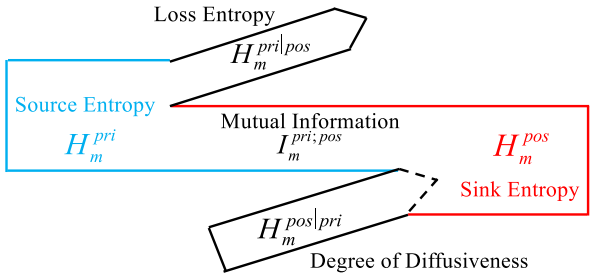

Fig. 3. The relationship between five types of CPs (sink entropy, source entropy, loss entropy, degree of diffusiveness, and mutual information).

Since $I_m^{pri;pos}$ is a convex function with $\mathbf{P}_m^{pri}$ as its independent variable, it is always possible to find a $\mathbf{P}_m^{pri}$ to maximize $I_m^{pri;pos}$, namely C_m, which indicates the maximum amount of information able to be transmitted between brain regions. For more details about the iterative computation of C_m, refer to the [20], and [21].

h) Limited entropy: According to the literature, equilibrium refers to the state of a biological system that does not evolve over time, and is used to describe the long-term dynamics of that system [31]. This study attempts to calculate the amount of information contained within each EEG subsystem when it reaches the equilibrium state, namely limited entropy.

$$\mathbf{P}_m^{pos|pri}\mathbf{S}_m = \mathbf{S}_m \tag{26}$$

$$\sum_{i=1}^{n} S_m^i = 1 \quad (S_m^i \geq 0) \tag{27}$$

$$H_m^{\infty} = -\sum_{i=1}^{n}\sum_{j=1}^{n} S_m^i p_m\left(l_j^{pos}|l_i^{pri}\right)\log p_m\left(l_j^{pos}|l_i^{pri}\right) \tag{28}$$

where $\mathbf{S}_m = \left[S_m^1, \ldots, S_m^i, \ldots, S_m^n\right]^T$, and $\mathbf{S}_m$ represents the power distribution of all EEG leads when the m^{th} subsystem reaches its equilibrium state.

2) CP Distribution Evaluation at Each EEG Frequency Band: As can be seen, a total of 8 CPs, namely H_m^{pri}, H_m^{pos}, $H_m^{pri|pos}$, $H_m^{pos|pri}$, $I_m^{pri;pos}$, $H_m^{pri,pos}$, C_m, and H_m^{∞}, can be derived from the m^{th} EEG subsystem. Since each subsystem has its own oscillatory frequency f_m, the DIs for each type of CP, including mean, variance, skewness and kurtosis [32], can be easily calculated within each EEG frequency band. Therefore, a total of 32 CP DIs can be obtained within each EEG signal band for further analysis.

E. Statistical Tests

The Jarque-Bera normality test was performed for each CP DI at the significance level of 0.05. Since almost all of the CP DIs are not normally distributed, the Wilcoxon rank-sum test was implemented to assess differences of these CP DIs between PD patients and HC. p values less than 0.05 after Bonferroni correction were considered significant.

F. Classification

In this study, a total of 32 CP DIs derived from each EEG frequency band were used to differentiate between PD patients and HC, by ten commonly used classifiers: Bayes Net (BYN), Naive Bayes (NB), support vector machine (SVM), Bagging (BG), J48, simple logistic (SL), k-nearest neighbor (KNN), Adaboost (AB), random forest (RF) and light gradient boosting machine (LGB) [33], [34], [35], [36], [37], [38], [39], [40], [41]. These classifiers are built into the well-known software Weka [42]. In addition, 10-fold cross-validation was employed, and the corresponding accuracy, precision, recall, and AUC were calculated as indices to evaluate the two-subject group differentiation [43]. Finally, the L2-norm sparse constraint was implemented on the CP DIs in order to prevent model overfitting.

Furthermore, two additional data processing procedures were applied for comparison: (1) 8 CPs (H^{pri}, H^{pos}, $H^{pri|pos}$, $H^{pos|pri}$, $I^{pri;pos}$, $H^{pri,pos}$, C and H^{∞}) were calculated directly from each EEG frequency band, respectively. Since these CPs are not derived from decomposed EEG subsystems, the unparallel communication model (UCM) was adopted for comparison. (2) Three types of BN were first constructed based on PC, PLV and GC. Then, corresponding topological attributes were extracted for the two-subject group classification [44], [45], [46].

III. Results

Fig. 4 shows the means and standard deviations of CP DIs for PD and HC. We found that out of the total 32 DIs in each EEG frequency band, 21, 18, 23 and 27 DIs were significant for detection of PD patients at delta, theta, alpha and beta EEG frequency bands, respectively, which convincingly demonstrates the effectiveness of our proposed approach and the feasibility of simultaneously investigating MIT of EEG signals in the space-time-frequency domain.

Fig. 5 illustrates the classification performance of PCM, UCM and BN for two-subject group differentiation at each EEG frequency band. The average accuracy, precision, recall and AUC of PCM for the ten commonly used classifiers at the delta frequency band were 0.937, 0.938, 0.937 and 0.955, respectively; at the theta band were 0.895, 0.899, 0.893 and 0.905, respectively; at the alpha band were 0.847, 0.849, 0.850 and 0.902, respectively; and at the beta band were 0.918, 0.919, 0.921 and 0.940, respectively. PCM showed a significantly stronger ability to differentiate between the two groups than UCM, PC-based BN, or PLV-based BN. Although its classification ability was not significantly different from that of GC-based BN, computation time was much shorter. For more details, refer to the discussion.

In sum, it is more reasonable and effective for PCM to reveal the MIT of EEG signals simultaneously in the space-time-frequency domain, rather than UCM or BN, both of which only include the MIT in the spato-temporal domain or spatial domain. Finally, Fig. 5 illustrates all the classification performance values for ten commonly used classifiers to differentiate the two subject groups. The mean and standard

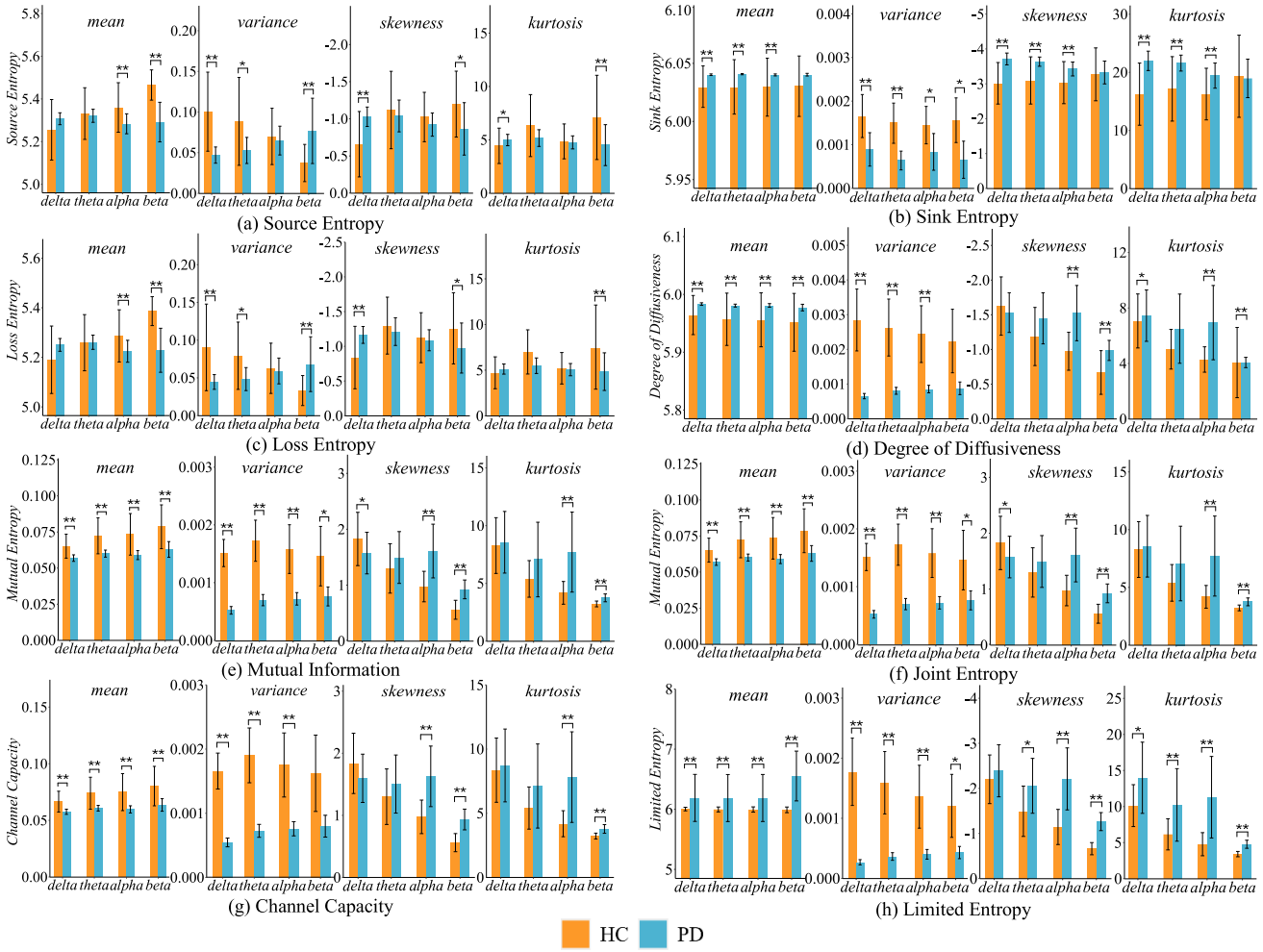

Fig. 4. The means and standard deviations of CP DIs at each EEG frequency band for PD and HC (After Bonferroni correction, $^{*}p < 0.05$, $^{**}p < 0.01$).

deviation of their AUC, precision and recall values are also shown in the Table II in the Appendix.

IV. Discussion

The use of network science to analyze MIT has become a research hotspot in recent years, since much research has already shown that signals are not independent of each other, but affect each other through information interaction [47]. However, as mentioned in the introduction, this method still has some deficiencies. Therefore, in this paper, we proposed a new approach, namely DMD-based PCM, to verify the feasibility of simultaneously analyzing MIT in the space-time-frequency domain. Then, we took multidimensional EEG signals as an example to illustrate our proposed method.

This paper regards all brain regions as both senders and receivers in the communication model. A TPM was used to represent the communication channels, describing how information is transmitted from one region to another over time (including within the same brain region). It is worth noting that the autocorrelation coefficient (or normalized phase-locking value) of an EEG signal is always equal to 1. This is one of the main reasons why the traditional BN method generally does not take into account self-loops of network nodes; that is, it cannot describe the influence of a brain region on itself over time. However, this is clearly not a comprehensive description of brain activity, and even contradicts much of the previous literature. For example, biological neuron models are mathematical descriptions of cells in the nervous system that generate sharp electrical potentials across their membranes. Although biological neuron models contain many subtypes, without exception, all such models show that the current discharge of a neuron is highly related to its own previous voltage level [14]. In addition, the autoregressive model, which indicates that the current amplitude of an EEG signal can be predicted by a linear combination of its previous amplitudes, is the most widely accepted one for EEG analysis [15], [16]. Therefore, no matter from the cellular or macro level, the neural activities of the brain are temporally correlated; the current activation state of a neuron is impossible to separable from its previous states, which means that temporal information must be taken into account in studying MIT.

In engineering, there are many subtypes of communication models. Since much previous literatures have demonstrated that the brain is a complex and large-scale system composed of many subsystems [8], [9], [19], this paper adopted the PCM. Thus, investigation of how information is transmitted within EEG subsystems provides a more complete frame of brain activity. This study selected DMD to decompose the

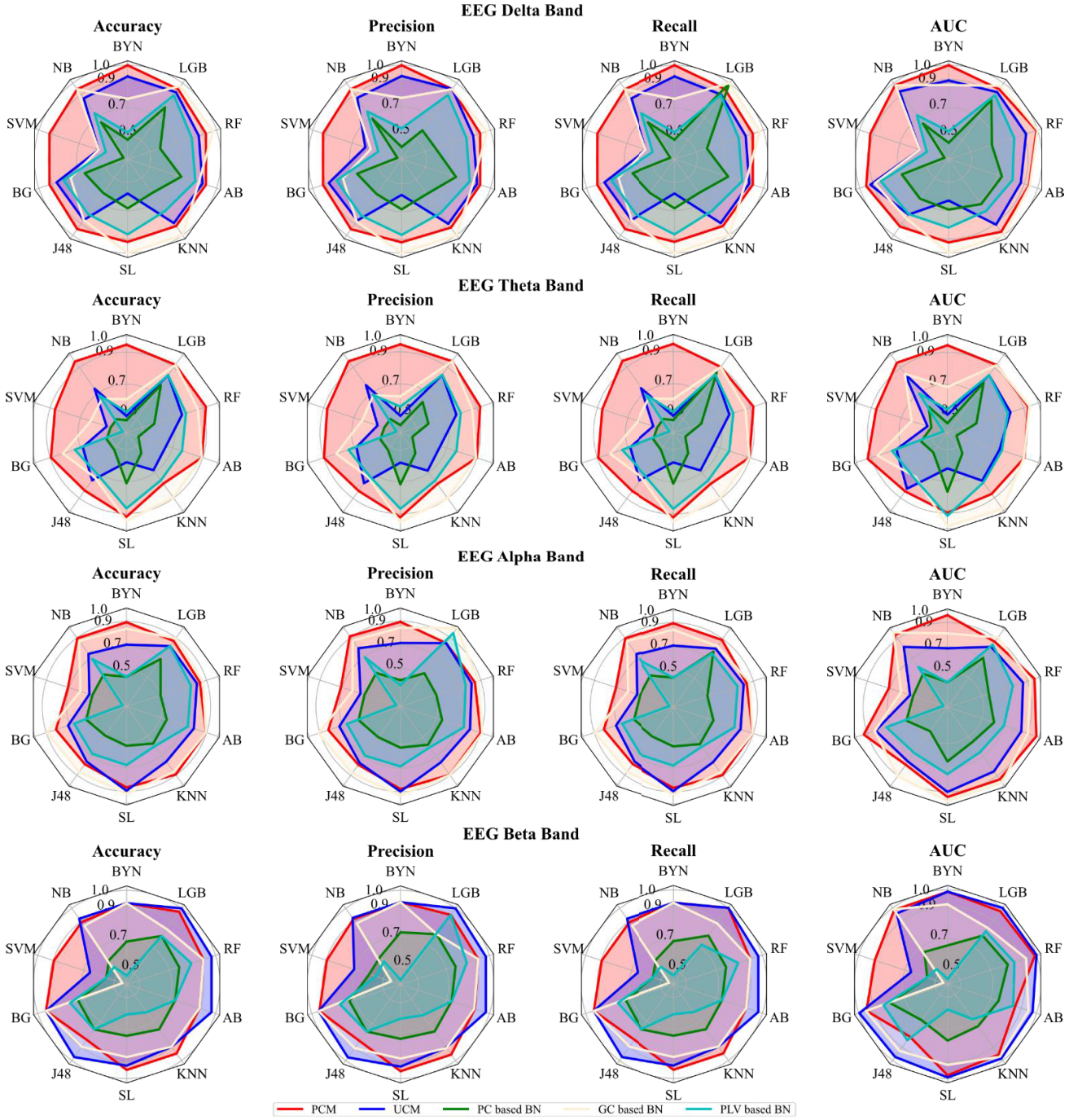

Fig. 5. Classification performance between PD and HC by PCM, UCM, PC-based BN, GC-based BN and PLV-based BN, at each EEG frequency band, respectively.

EEG signals into subsystems, for the following reasons: (1) DMD has been demonstrated to be able to make full use of EEG information to capture potential subsystems of the brain, so-called DMs. (2) DMD does not require any prior assumptions, such as determined system equations, to process the EEG data. Thus, it is a powerful data-driven approach, especially suitable for processing physiological signals with high dimensionality and complexity [17], [18]. (3) Each DM has its own inherent frequency, which provides the basis for the use of PCM to investigate EEG signals, since, in PCM, different frequency-specific signals are conveyed via different communication subsystems. Furthermore, the TPM derived from DMD can indicate spatio-temporal information transmission patterns within and between EEG signals in each subsystem. Thus, DMD provides the foundation to simultaneously analyze inter-series and intra-series information transitions of EEG signals in each dynamic subsystem, namely concurrently assessing MIT of EEG signals in the space-time-frequency domain.

In this study, eight types of CPs were utilized to describe the brain information transition: (1) H_m^{pri}, H_m^{pos}, $H_m^{pri|pos}$, $H_m^{pos|pri}$ and $I_m^{pri;pos}$ are the most commonly used CPs to evaluate how information is transferred from senders to receivers in the communication model; their relationship is

shown in Fig. 3. The information content of H_m^{pri} and H_m^{pos} is usually not equal, because some of the H_m^{pri} emitted from the sender, that is $H_m^{pri|pos}$, does not eventually arrive at the receiver. In our case, this parameter might indicate the amount of information sent from brain regions but is eventually delivered to other physiological systems. On the other hand, $H_m^{pos|pri}$ represents the information arriving at the receiver which does not come from the sender. In our case, this parameter might indicate that the information arriving at brain regions comes from other physiological systems during information transmission. In this way, our approach may be more consistent with physiological facts than the traditional BN method. The brain is connected to the peripheral nervous system, which is responsible for transmitting information to the whole body, and simultaneously collecting information from the body, coordinating the brain with all organs of the body. Even when a person is at rest, the messages sent by brain regions cannot only travel between them. Some of the information must also be delivered to the peripheral nervous system, which controls basic physiological activities such as breathing and heartbeat. At the same time, information from the peripheral nervous system is also fed back to the brain in real time [48], [49]. However, previous research has only regarded the brain as a closed system, which is not very scientific. In this model, it is possible to use $H_m^{pri|pos}$ and $H_m^{pos|pri}$ to investigate such mechanisms. Actually, it is the exactly amount of information, $I_m^{pri;pos}$, transmitted between brain regions during communication process. (2) Channel capacity C_m is the most widely used CP in the communication model, describing the maximum amount of information that can be transmitted from the sender to the receiver [20], [50]. This study used this parameter to measure the maximum information transmission capacity of the brain, and to investigate whether diseases can significantly change this capacity. (3) Equilibrium, meaning state does not vary over time, reveals the long-term dynamics of a biological system. In fact, there have been many studies on equilibrium in physiological systems, involving sleep, gait, and circulatory system, etc., which have demonstrated its great significance for identification of diseases [31], [51], [52]. However, no study has been conducted so far on the equilibrium state of brain information transmission. Thus, this study has proposed and explored the parameter of limited entropy, namely H_m^{∞}, when the information transmission process is being an equilibrium.

We have some comments on the results, as follows: (1) This paper does not view the EEG signals as a closed system, but as an open system that constantly interacts with other physiological systems. As shown in Fig. 3, the influence of the brain on other physiological systems might be expressed as loss of entropy, while the influence of other physiological systems on the brain might be manifested in degree of diffusiveness. It is apparent from Fig. 4 (c) that the average loss entropy in PD patients is significantly lower than in the HC group, indicating that the brains of PD patients exhibit decreased control over the activities of other physiological systems. In contrast, as shown in Fig. 4 (d), the average degree of diffusion in PD patients is significantly higher than in the HC group, indicating that in PD patients, other physiological systems send a large amount of information to the brain, which may be due to a variety of whole-physiological symptoms in PD patients [53]. In addition, it can be found from Fig. 4 (a), (b) and (f) that the amount of information in the brains of PD patients increases over time. These findings are also consistent with much of the previous literature that PD patients show cognitive overload [54]. Also considering Fig. 4 (c) and (d), one possible reason is that the brains of PD patients are unable to properly process and integrate abnormal information received from other physiological systems. Instead, a lot of faulty information is generated in their neural circuits, thus resulting in cognitive overload, which may in turn also further hinder the brain's ability to control peripheral physiological systems. (2) We also introduced the channel capacity parameter to estimate the maximum information transmission capacity of the brain (Fig. 4 (g)), and found that the value of this parameter in PD patients was significantly lower than that in healthy people. This finding is supported by a lot of previous medical literature. For example, Du et al. showed that the information processing ability of PD patients was significantly decreased due to the decrease of dopamine and precipitation of α synuclein oligomers, and there is even disorganized neuronal cross-talk between these brain circuits [55]. (3) This study also introduced the concept of limited entropy, which can be used to characterize the chaotic state of the brain over a long period. Many previous studies have shown that the physiological mechanisms of ill or aging individuals are in a more disordered state [56]. As can be seen from Fig. 4 (h), the average limited entropy of PD patients is significantly higher than that of the HC group, which not only indicates that PD significantly increases the degree of brain disorder, but also explains the cause of extensive cognitive conflict in PD patients from a physical perspective. (4) Research on the variability of physiological parameters has always been an important means to understand the biological mechanisms of diseases. For example, a large literature has shown that the variability of electrocardiogram and gait rhythm signals in HC groups is greater than in pathological groups, which indicates that healthy physiological systems have strong plasticity [57], [58]. Therefore, variance, skewness and kurtosis were used in this study to evaluate the variation of CPs. The results showed that for most of the extracted CPs, HC had greater variability than PD patients, which suggests that their brains show stronger plasticity.

In this study, the PCM parameters in EEG signals extracted by each individual were also tested by Spearman correlation with their UPDRS scale scores. The results showed that after Bonferroni correction, a total of four parameters in the alpha band and three in the beta EEG band were significantly correlated. Previous literature has shown that many later-stage PD patients have cognitive impairment, and the alpha and beta bands of their EEG signals best represent their cognitive state [59]. In addition, the parameter among these seven with the largest absolute value is channel capacity, measured in the EEG alpha band. This parameter fully indicates that with the aggravation of the disease, the maximum transmission

TABLE I
A COMPARISON OF THREE METHODOLOGIES

	Our Method	Network Analysis	Tensor Analysis
Can this method represent MS in the space-time-frequency domain?	**Yes (DMD)**	No	Yes
Does this approach reveal MIT?	**Yes (DMD)**	Yes (Network)	No
Does this method use quantitative parameters to measure MIT?	**Yes (PCM)**	Yes (Topology)	No

capacity of information inside their brain decreases significantly.

In order to verify the effectiveness of our proposed method, we provided two comparisons, namely UCM and BN, which only reveal the information transition patterns of multidimensional EEG signals from space-time and spatial perspectives, respectively. First, we used UCM to distinguish two-subject groups; that is, the EEG signals were not decomposed into subsystems for analysis. The results show that compared with UCM, PCM significantly enhanced the recognition accuracy. This comparison confirms the previous conclusion to some extent – that is, the brain is composed of multiple subsystems, each with its own properties. Second, we used the traditional BN method for comparison. As shown in Fig. 5, the classification performance of PCM was significantly higher than that of PC- and PLV-based BN. Moreover, with GC-based BN, PCM showed no significant difference in classification ability. However, GC-based BN requires quite a lot of computing time. For example, our approach required only 195.46 seconds to extract the CPs of a PD patient, but 28,062.78 seconds to construct a GC BN. Thus, our proposed method not only has high classification accuracy, but also saves much computation cost, which provides the possibility for future big data processing on EEG signals. Thus, our proposed method not only saves computation time, but also fully reveals the information transition of multi-dimensional EEG signals from a space-time-frequency perspective.

It has been widely recognized that classic methods for processing MS such as empirical mode decomposition, multivariate empirical mode decomposition, multivariate empirical wavelet transform, wavelet transform, tensor decomposition, independent component analysis, multivariate Fourier-Bessel series expansion based empirical wavelet transform, and multivariate iterative filtering are effective [60], [61], [62], [63], [64], [65]. It should be noted that these methods mainly focus on the decomposition of MS, including its decomposition into the space-time-frequency domain, which on the surface is similar to our research, but in fact is completely different. Based on previous research, MIT can only achieve this by combining these methods with complex network techniques together. (Here, we point out that although combinations of the above approaches can be used to describe information transmission among MS to some extent, they still do not manifest how MIT operates in these three domains simultaneously). Specifically, we first used those methods to decompose MS, and then employed their corresponding decomposition components to construct brain network, and finally extracted a set of common topological parameters (such as clustering coefficients, etc.) from the resulting brain networks for disease classification [66]. The mean and standard deviation of the AUC, precision and recall values for ten commonly used

TABLE II
MEAN AND STANDARD DEVIATION OF CLASSIFICATION PERFORMANCE FOR OUR DEVELOPED AND TRADITIONAL METHODS

EEG Band	Methods	Accuracy		Precision		Recall		AUC	
		Mean	SD	Mean	SD	Mean	SD	Mean	SD
EEG alpha band	**PCM**	**0.84**	**0.06**	**0.77**	**0.25**	**0.85**	**0.06**	**0.89**	**0.09**
	UCM	0.74	0.09	0.69	0.23	0.74	0.09	0.78	0.10
	PC-based BN	0.54	0.05	0.47	0.15	0.55	0.07	0.56	0.06
	GC-based BN	0.85	0.08	0.79	0.26	0.84	0.08	0.87	0.10
	PLV-based BN	0.67	0.08	0.62	0.22	0.66	0.07	0.67	0.09
	WT	0.61	0.04	0.55	0.18	0.61	0.04	0.64	0.05
	EMD	0.63	0.06	0.59	0.19	0.64	0.06	0.66	0.07
	EEMD	0.57	0.05	0.52	0.17	0.57	0.05	0.59	0.06
	EWT	0.57	0.04	0.52	0.17	0.57	0.04	0.60	0.06
	ICA	0.54	0.03	0.50	0.16	0.54	0.03	0.55	0.04
	TD	0.59	0.08	0.54	0.19	0.59	0.08	0.59	0.08
EEG beta band	**PCM**	**0.91**	**0.03**	**0.83**	**0.26**	**0.91**	**0.04**	**0.93**	**0.06**
	UCM	0.91	0.09	0.83	0.27	0.91	0.09	0.95	0.09
	PC-based BN	0.71	0.07	0.65	0.21	0.71	0.07	0.72	0.07
	GC-based BN	0.84	0.13	0.76	0.27	0.85	0.13	0.88	0.14
	PLV-based BN	0.67	0.12	0.62	0.24	0.66	0.11	0.70	0.15
	WT	0.58	0.05	0.52	0.17	0.58	0.05	0.62	0.06
	EMD	0.62	0.07	0.57	0.19	0.62	0.07	0.61	0.07
	EEMD	0.58	0.06	0.53	0.18	0.58	0.06	0.56	0.06
	EWT	0.64	0.05	0.60	0.19	0.64	0.05	0.67	0.05
	ICA	0.52	0.01	0.48	0.15	0.52	0.01	0.53	0.03
	TD	0.73	0.07	0.68	0.22	0.73	0.07	0.75	0.09
EEG delta band	**PCM**	**0.92**	**0.03**	**0.84**	**0.26**	**0.92**	**0.03**	**0.94**	**0.03**
	UCM	0.81	0.13	0.74	0.26	0.81	0.13	0.84	0.12
	PC-based BN	0.61	0.12	0.53	0.20	0.63	0.16	0.63	0.13
	GC-based BN	0.85	0.14	0.77	0.28	0.86	0.14	0.89	0.14
	PLV-based BN	0.74	0.13	0.68	0.24	0.74	0.13	0.75	0.12
	WT	0.85	0.06	0.77	0.25	0.85	0.06	0.86	0.06
	EMD	0.80	0.08	0.73	0.24	0.80	0.08	0.82	0.08
	EEMD	0.63	0.12	0.57	0.21	0.63	0.12	0.65	0.13
	EWT	0.60	0.07	0.55	0.18	0.60	0.07	0.59	0.07
	ICA	0.54	0.02	0.51	0.16	0.53	0.02	0.55	0.03
	TD	0.68	0.14	0.62	0.24	0.68	0.14	0.68	0.15
EEG theta band	**PCM**	**0.90**	**0.04**	**0.82**	**0.26**	**0.90**	**0.04**	**0.91**	**0.02**
	UCM	0.68	0.11	0.62	0.22	0.68	0.11	0.71	0.12
	PC-based BN	0.56	0.09	0.50	0.17	0.57	0.11	0.58	0.11
	GC-based BN	0.81	0.12	0.74	0.26	0.80	0.12	0.85	0.11
	PLV-based BN	0.71	0.13	0.65	0.24	0.71	0.13	0.73	0.14
	WT	0.64	0.07	0.59	0.20	0.64	0.07	0.68	0.11
	EMD	0.75	0.08	0.69	0.23	0.75	0.08	0.78	0.10
	EEMD	0.74	0.08	0.68	0.22	0.74	0.08	0.77	0.11
	EWT	0.59	0.05	0.54	0.18	0.59	0.05	0.63	0.06
	ICA	0.53	0.02	0.50	0.16	0.53	0.02	0.53	0.04
	TD	0.61	0.08	0.56	0.19	0.61	0.08	0.62	0.09

Note: WT: Wavelet Transform; EMD: Empirical Mode Decomposition; EEMD: Ensemble Empirical Mode Decomposition; EWT: Empirical Wavelet Transform; ICA: Independent Component Analysis: TD: Tensor Decomposition.

classifiers to differentiate the two subject groups based on the above approaches are also shown in the Table II in the Appendix. In addition, we used two additional data sets (patients with epilepsy and Alzheimer's disease, and HC) to fully verify the validity of our approach. The epilepsy data was classified using a public data set of 1800 EEG recordings during seizures and 1800 EEG recordings during normal conditions. For Alzheimer's disease, we used a data set collected by hospitals in Sichuan Provincial Province (including 45 Alzheimer's patients and 45 healthy controls). The above comparisons once again verify that our method was at least not significantly inferior to the above traditional methods for distinguishing the disease group from the HC.

Possible follow-up work may be as follows: (1) As mentioned above, PD patients experience not only brain dysfunction but also a variety of whole-physiological symptoms, including motor and non-motor symptoms. This is mainly because in addition to the substantia nigra and locus coeruleus, PD also affects other areas such as the hypothalamus, dorsal vagus nucleus, sympathetic ganglion and adrenal medulla [67]. For example, Hilton et al. found that α-synuclein deposition already occurs in the nerve fibers and ganglia in the submucosal layer of the stomach, duodenum and colon of PD patients as early as 8 years before the onset of symptoms [68]. In addition, pathological studies have also confirmed the presence of Lewy body changes in the cardiac sympathetic nerve fibers and ganglia, suggesting that PD patients may develop cardiac sympathetic nerve disorders in the early stage [69]. In our later studies, we plan to use our approach to investigate the EEG signals of early-stage PD patients. Since our proposed approach treats the brain as an open, rather than a closed system, it is possible that the newly developed parameters describing the neural information coming from the activities of the peripheral nervous system might be used to better identify early-stage patients. (2) Many patients with neurodegenerative diseases may present with Parkinsonian features (e.g., Parkinson-plus syndromes). In follow-up research, we also hope to adopt our approach to investigate the differences in DMD-based PCM parameter values between PD patients and those with Parkinsonian syndrome.

V. Conclusion

In this study, a DMD-based PCM model is developed, which proves the feasibility of assessing MIT in space-time-frequency domain simultaneously for the first time, while traditional approaches cannot achieve this. Furthermore, this study demonstrates that MIT in space-time-frequency domain is quite different from MS decomposition in these three domains. In addition, our proposed approach does not treat MS as a closed system, but rather as an open system, which may represent information from or transmitted to the external environment. Finally, compared with traditional methods, our proposed approach can not only help solve practical problems in various fields, such as disease detection, but also reveals many new phenomena behind MS that have not yet been discovered. In sum, we propose a new approach, which can comprehensively quantify the information transmission of MS in multi-domain, thus providing new possibilities for many applications in the future.

Appendix

See Tables I and II.

References

[1] L. Lacasa, V. Nicosia, and V. Latora, "Network structure of multivariate time series," *Sci. Rep.*, vol. 5, no. 1, p. 15508, Oct. 2015.

[2] Z. Gao, M. Small, and J. Kurths, "Complex network analysis of time series," *Europhys. Lett.*, vol. 116, no. 5, p. 50001, 2016.

[3] J. Zhang, J. Sun, X. Luo, K. Zhang, T. Nakamura, and M. Small, "Characterizing pseudoperiodic time series through the complex network approach," *Phys. D, Nonlinear Phenomena*, vol. 237, no. 22, pp. 2856–2865, Nov. 2008.

[4] M. Stephen, C. Gu, and H. Yang, "Visibility graph based time series analysis," *PLoS ONE*, vol. 10, no. 11, Nov. 2015, Art. no. e0143015.

[5] J. I. Deza, M. Barreiro, and C. Masoller, "Inferring interdependencies in climate networks constructed at inter-annual, intra-season and longer time scales," *Eur. Phys. J. Special Topics*, vol. 222, no. 2, pp. 511–523, Jun. 2013.

[6] J. Tang, Y. Wang, H. Wang, S. Zhang, and F. Liu, "Dynamic analysis of traffic time series at different temporal scales: A complex networks approach," *Phys. A, Stat. Mech. Appl.*, vol. 405, pp. 303–315, Jul. 2014.

[7] M. Weis, F. Romer, M. Haardt, D. Jannek, and P. Husar, "Multi-dimensional space-time-frequency component analysis of event related EEG data using closed-form PARAFAC," in *Proc. IEEE Int. Conf. Acoust., Speech Signal Process.*, Apr. 2009, pp. 349–352.

[8] J. Lunze, "Stability analysis of large-scale systems composed of strongly coupled similar subsystems," *Automatica*, vol. 25, no. 4, pp. 561–570, Jul. 1989.

[9] H. Niyigena Ingabire et al., "Analysis of ECG signals by dynamic mode decomposition," *IEEE J. Biomed. Health Informat.*, vol. 26, no. 5, pp. 2124–2135, May 2022.

[10] A. Biasiucci, B. Franceschiello, and M. M. Murray, "Electroencephalography," *Current Biology*, vol. 29, no. 3, pp. R80–R85, Feb. 2019.

[11] M. Jalili and M. G. Knyazeva, "EEG-based functional networks in schizophrenia," *Comput. Biol. Med.*, vol. 41, no. 12, pp. 1178–1186, Dec. 2011.

[12] H. Deng, G. Qian, Y. Zhang, C. Hu, Y. Liu, and H. Li, "Emotional analysis and recognition based on EEG brain network," in *Proc. 8th Int. Conf. Adv. Cloud Big Data (CBD)*, Dec. 2020, pp. 56–61.

[13] N. Nicolaou and J. Georgiou, "Neural network-based classification of anesthesia/awareness using Granger causality features," *Clinical EEG Neuroscience*, vol. 45, no. 2, pp. 77–78, Apr. 2014.

[14] A. L. Hodgkin and A. F. Huxley, "A quantitative description of membrane current and its application to conduction and excitation in nerve," *J. Physiol.*, vol. 117, no. 4, pp. 500–544, Aug. 1952.

[15] Y. Zhang, B. Liu, X. Ji, and D. Huang, "Classification of EEG signals based on autoregressive model and wavelet packet decomposition," *Neural Process. Lett.*, vol. 45, no. 2, pp. 365–378, Apr. 2017.

[16] A. Schlögl and G. Supp, "Analyzing event-related EEG data with multivariate autoregressive parameters," in *Progress in Brain Research*, vol. 159, C. Neuper and W. Klimesch, Eds. Amsterdam, The Netherlands: Elsevier, 2006, pp. 135–147.

[17] B. W. Brunton, L. A. Johnson, J. G. Ojemann, and J. N. Kutz, "Extracting spatial–temporal coherent patterns in large-scale neural recordings using dynamic mode decomposition," *J. Neurosci. Methods*, vol. 258, pp. 1–15, Jan. 2016.

[18] J. N. Kutz, S. L. Brunton, B. W. Brunton, and J. L. Proctor, *Dynamic Mode Decomposition: Data-Driven Modeling of Complex Systems*. Philadelphia, PA, USA: SIAM, 2016.

[19] S. Liu et al., "Brain network analysis by stable and unstable EEG components," *IEEE J. Biomed. Health Informat.*, vol. 25, no. 4, pp. 1080–1092, Apr. 2021.

[20] F. M. Reza, *An Introduction to Information Theory*. North Chelmsford, MA, USA: Courier Corporation, 1994, pp. 2–109.

[21] R. M. Gray, *Entropy and Information Theory*. Berlin, German: Springer, 2011, pp. 22–29.

[22] C. E. Shannon, "A mathematical theory of communication," *ACM SIGMOBILE Mobile Comput. Commun. Rev.*, vol. 5, no. 1, pp. 3–55, Jan. 2001.

[23] J. D. Touch, "Parallel communication," in *Proc. IEEE INFOCOM Conf. Comput. Commun.*, Jun. 1993, pp. 505–512.

[24] W. Poewe et al., "Parkinson disease," *Nature Rev. Disease Primers*, vol. 3, Mar. 2017, Art. no. 17013.

[25] N. Li et al., "Brain network topology and future development of freezing of gait in Parkinson's disease: A longitudinal study," *J. Neurol.*, vol. 269, no. 5, pp. 2503–2512, Oct. 2021.

[26] V. J. Geraedts et al., "Clinical correlates of quantitative EEG in Parkinson disease: A systematic review," *Neurology*, vol. 91, no. 19, pp. 871–883, Nov. 2018.

[27] K. T. E. O. Dubbelink et al., "Disrupted brain network topology in Parkinson's disease: A longitudinal magnetoencephalography study," *Brain*, vol. 137, pp. 197–207, Jan. 2014.

[28] N. Bigdely-Shamlo, T. Mullen, C. Kothe, K.-M. Su, and K. A. Robbins, "The PREP pipeline: Standardized preprocessing for large-scale EEG analysis," *Frontiers Neuroinform.*, vol. 9, p. 16, Jun. 2015.

[29] J. L. Proctor and P. A. Eckhoff, "Discovering dynamic patterns from infectious disease data using dynamic mode decomposition," *Int. Health*, vol. 7, no. 2, pp. 139–145, Mar. 2015.

[30] J. H. Tu, C. W. Rowley, D. M. Luchtenburg, S. L. Brunton, and J. N. Kutz, "On dynamic mode decomposition: Theory and applications," *J. Comput. Dyn.*, vol. 1, no. 2, pp. 391–421, Nov. 2013.

[31] C. Wang, S. A. Alvarez, C. Ruiz, and M. Moonis, "Computational modeling of sleep stage dynamics using Weibull semi-Markov chains," in *Proc. Int. Conf. Health Informat.*, Barcelona, Spain, Feb. 2013, pp. 122–130.

[32] M. K. Cain, Z. Zhang, and K.-H. Yuan, "Univariate and multivariate skewness and kurtosis for measuring nonnormality: Prevalence, influence and estimation," *Behav. Res. Methods*, vol. 49, no. 5, pp. 1716–1735, Oct. 2017.

[33] R. K. Sharma, V. Sugumaran, H. Kumar, and M. Amarnath, "A comparative study of naïve Bayes classifier and Bayes net classifier for fault diagnosis of roller bearing using sound signal," *Int. J. Decis. Support Syst.*, vol. 1, no. 1, pp. 115–129, Jan. 2015.

[34] C. C. Chang and C. J. Lin, "LIBSVM: A library for support vector machines," *ACM Trans. Intell. Syst. Technol.*, vol. 2, no. 3, pp. 1–27, 2011.

[35] A. Mosavi, F. S. Hosseini, B. Choubin, M. Goodarzi, A. A. Dineva, and E. R. Sardooi, "Ensemble boosting and bagging based machine learning models for groundwater potential prediction," *Water Resour. Manag.*, vol. 35, no. 1, pp. 23–27, Jan. 2021.

[36] N. Bhargava, G. Sharma, R. Bhargava, and M. Mathuri, "Decision tree analysis on J48 algorithm for data mining," *Int. J. Adv. Res. Comput. Sci. Softw. Eng.*, vol. 3, no. 6, Jun. 2013, pp. 1114–1119.

[37] K. Meganathan, "Sample size determination in simple logistic regression: Formula versus simulation," Ph.D. thesis, School Math. Sci., Univ. Cincinnati, Cincinnati, OH, USA, 2021.

[38] L. E. Peterson, "K-nearest neighbor," *Scholarpedia*, vol. 4, no. 2, p. 1883, 2009.

[39] W. Hu, W. Hu, and S. Maybank, "AdaBoost-based algorithm for network intrusion detection," *IEEE Trans. Syst., Man, Cybern. B, Cybern.*, vol. 38, no. 2, pp. 577–583, Apr. 2008.

[40] A. Liaw and M. Wiener, "Classification and regression by random forest," *R News*, vol. 2, no. 3, pp. 18–22, Dec. 2002.

[41] G. Ke et al., "LightGBM: A highly efficient gradient boosting decision tree," in *Proc. NeurIPS*, vol. 30, Long Beach, CA, USA, Dec. 2017, pp. 1–9.

[42] G. Holmes, A. Donkin, and I. H. Witten, "WEKA: A machine learning workbench," in *Proc. ANZIIS Austral. New Zealnd Intell. Inf. Syst. Conf.*, 1994, pp. 357–361.

[43] T. Fushiki, "Estimation of prediction error by using K-fold cross-validation," *Statist. Comput.*, vol. 21, no. 2, pp. 137–146, Apr. 2011.

[44] T. L. Richards, V. W. Berninger, K. Yagle, R. D. Abbott, and D. Peterson, "Brain's functional network clustering coefficient changes in response to instruction (RTI) in students with and without reading disabilities: Multileveled reading brain's RTI," *Cogent Psychol.*, vol. 5, no. 1, Dec. 2018, Art. no. 1424680.

[45] Q. Yu et al., "Altered topological properties of functional network connectivity in schizophrenia during resting state: A small-world brain network study," *PLoS ONE*, vol. 6, no. 9, Sep. 2011, Art. no. e25423.

[46] P. McColgan et al., "Selective vulnerability of rich club brain regions is an organizational principle of structural connectivity loss in Huntington's disease," *Brain*, vol. 138, no. 11, pp. 3327–3344, Nov. 2015.

[47] D. S. Bassett and M. S. Gazzaniga, "Understanding complexity in the human brain," *Trends Cognit. Sci.*, vol. 15, no. 5, pp. 200–209, May 2011.

[48] D. S. Bassett and O. Sporns, "Network neuroscience," *Nature Neurosci.*, vol. 20, no. 3, pp. 353–364, Feb. 2017.

[49] J. J. Lynch and D. A. Paskewitz, "On the mechanisms of the feedback control of human brain-wave activity," in *Mind/Body Integration: Essential Readings in Biofeedback*, E. Peper, S. Ancoli, and M. Quinn, Eds. Boston, MA, USA: Springer, 1979, pp. 325–340.

[50] R. E. Blahut, "Computation of channel capacity and rate-distortion functions," *IEEE Trans. Inf. Theory*, vol. IT-18, no. 4, pp. 460–473, Jul. 1972.

[51] L. Wallard, G. Dietrich, Y. Kerlirzin, and J. Bredin, "Effect of robotic-assisted gait rehabilitation on dynamic equilibrium control in the gait of children with cerebral palsy," *Gait Posture*, vol. 60, pp. 55–60, Feb. 2018.

[52] R. N. Pittman, "The circulatory system and oxygen transport," in *Regulation of Tissue Oxygenation*. San Rafael, CA, USA: Morgan & Claypool Life Sciences, 2011.

[53] J. Horsager, K. Knudsen, and M. Sommerauer, "Clinical and imaging evidence of brain-first and body-first Parkinson's disease," *Neurobiol. Disease*, vol. 164, Mar. 2022, Art. no. 105626.

[54] H. Onder and O. Ozyurek, "The impact of distinct cognitive dual-tasks on gait in Parkinson's disease and the associations with the clinical features of Parkinson's disease," *Neurological Sci.*, vol. 42, pp. 2775–2783, Jul. 2021.

[55] X. Du, X. Xie, and R. Liu, "The role of α-synuclein oligomers in Parkinson's disease," *Int. J. Mol. Sci.*, vol. 21, no. 22, p. 8645, Nov. 2020.

[56] F. Alu et al., "Entropy modulation of electroencephalographic signals in physiological aging," *Mech. Ageing Develop.*, vol. 196, Jun. 2021, Art. no. 111472.

[57] S. Järvelin-Pasanen, S. Sinikallio, and M. P. Tarvainen, "Heart rate variability and occupational stress—Systematic review," *Ind. Health*, vol. 56, no. 6, pp. 500–511, 2018.

[58] N. Herssens, E. Verbecque, A. Hallemans, L. Vereeck, V. Van Rompaey, and W. Saeys, "Do spatiotemporal parameters and gait variability differ across the lifespan of healthy adults? A systematic review," *Gait Posture*, vol. 64, pp. 181–190, Jul. 2018.

[59] K. Baik et al., "Implication of EEG theta/alpha and theta/beta ratio in Alzheimer's and lewy body disease," *Sci. Rep.*, vol. 12, no. 1, p. 18706, Nov. 2022.

[60] A. Anuragi, D. S. Sisodia, and R. B. Pachori, "Automated alcoholism detection using Fourier-Bessel series expansion based empirical wavelet transform," *IEEE Sensors J.*, vol. 20, no. 9, pp. 4914–4924, May 2020.

[61] K. Das et al., "Electroencephalogram based motor imagery brain computer interface using multivariate iterative filtering and spatial filtering," *IEEE Trans. Cogn. Developmental Syst.*, early access, Oct. 14, 2022.

[62] A. Bhattacharyya and R. B. Pachori, "A multivariate approach for patient-specific EEG seizure detection using empirical wavelet transform," *IEEE Trans. Biomed. Eng.*, vol. 64, no. 9, pp. 2003–2015, Sep. 2017.

[63] P. Gajbhiye, R. K. Tripathy, and R. B. Pachori, "Elimination of ocular artifacts from single channel EEG signals using FBSE-EWT based rhythms," *IEEE Sensors J.*, vol. 20, no. 7, pp. 3687–3696, Apr. 2020.

[64] M. T. Sadiq et al., "Motor imagery EEG signals decoding by multivariate empirical wavelet transform-based framework for robust brain–computer interfaces," *IEEE Access*, vol. 7, pp. 171431–17145, 2019.

[65] S. I. Khan and R. B. Pachori, "Automated detection of posterior myocardial infarction from vectorcardiogram signals using Fourier–Bessel series expansion based empirical wavelet transform," *IEEE Sensors Lett.*, vol. 5, no. 5, pp. 1–4, May 2021.

[66] X. Shao et al., "Analysis of functional brain network in MDD based on improved empirical mode decomposition with resting state EEG data," *IEEE Trans. Neural Syst. Rehabil. Eng.*, vol. 29, pp. 1546–1556, 2021.

[67] M. G. Cersosimo and E. E. Benarroch, "Central control of autonomic function and involvement in neurodegenerative disorders," *Handbook Clin. Neurology*, vol. 117, pp. 45–57, Jan. 2013.

[68] D. Hilton et al., "Accumulation of α-synuclein in the bowel of patients in the pre-clinical phase of Parkinson's disease," *Acta Neuropathologica*, vol. 127, no. 2, pp. 235–241, Feb. 2014.

[69] S. Orimo et al., "Degeneration of cardiac sympathetic nerve begins in the early disease process of parkinson's disease," *Brain Pathol.*, vol. 17, no. 1, pp. 24–30, Jan. 2007.